Pathway and energetics of xenon migration in uranium dioxide

Alexander E. Thompson and C. Wolverton

Phys. Rev. B **87**, 104105 — Published 11 March 2013

DOI: 10.1103/PhysRevB.87.104105

Pathway and energetics of xenon migration in uranium dioxide

Alexander E. Thompson* and C. Wolverton

Department of Materials Science & Engineering, Northwestern University, Evanston, Illinois 60208, USA

**e-mail: Alexander-thompson@northwestern.edu*

Abstract

Using a combination of Density Functional Theory (DFT), classical potentials, Molecular Dynamics (MD), and Nudged Elastic Band (NEB) calculations, we explore the diffusion of xenon in uranium dioxide (UO_2). We compare migration barriers of empirical potentials with DFT by performing NEB calculations and subsequently we use the DFT-validated empirical potentials to calculate vacancy clusters, with and without xenon, to determine the migration path and barrier of xenon in bulk UO_2. We find (i) two empirical potentials out of four tested agree qualitatively with DFT derived energetics for Schottky defect migration, (ii) through the use of molecular dynamics with empirical potentials, we have found a new path for the diffusion of xenon-tetravacancy clusters (Xe + 2 V_U + 2 V_O), (iii) this new path has an energy barrier significantly lower than previously reported paths by nearly 1 eV, (iv) we examine the physical contributions to the migration pathway and find the barrier is largely electrostatic and that xenon contributes very little to the barrier height, (v) once a uranium vacancy attaches to a xenon-Schottky defect, the resulting xenon-tetravacancy cluster is strongly bound, and (vi) like xenon in a tetravacancy, a xenon-double Schottky defect can diffuse in a concerted manor with a comparable barrier to xenon in a tetravacancy, but two of the oxygen vacancies are only weakly bound to the defect.

I. Introduction

In the nuclear fuel uranium dioxide (UO_2), xenon atoms are created during the decay process of uranium. Xenon is highly insoluble in UO_2 and coalesces into bubbles, swelling the material, degrading its properties, and causing it to fail.[1] An important component to a more complete understanding of how xenon coalesces into clusters is how the individual xenon atoms diffuse. Miekeley and Felix measured the activation barrier for xenon diffusion in stoichiometric UO_2,[2] by extracting diffusion coefficients between 950 and 1700 °C. For stoichiometric UO_2, they measure an activation energy of 3.9 ± 0.4 eV (Miekeley and Felix also found a large variation of activation energy with stoichiometry, but we concentrate on stoichiometric UO_2 in this work).[2] However, the atomistic mechanism of *how* individual xenon atoms diffuse in the lattice to form bubbles is still a subject of active research.

There exist many possibilities for the location of xenon in UO_2 and the pathways it can take for diffusion. One possibility is that xenon diffuses interstitially, however, the octahedral interstitial position in uranium dioxide is highly strained and, consequently, energetically unfavorable.[3] Another possibility is that xenon diffuses on either the cation or anion sublattice. Matzke et al. addressed this possibility through a series of experiments.[4] By adding trivalent dopants to UO_2, vacancies were introduced into the oxygen sublattice, speeding diffusion among oxygen sites. Similarly, pentavalent dopants were added to UO_2 to produce vacancies in the uranium sublattice. However, xenon diffusion was not aided by either set of dopants. These results suggest that xenon atoms do not diffuse solely in either the cation or anion sublattice[5], instead diffusing in a cluster of vacancies.

The smallest, charge neutral group of vacancies in UO_2 is a Schottky defect cluster (SD). A SD is a very favorable site for xenon. For example, if xenon occupied an interstitial site (9.7 eV / Xe

atom), it would be energetically favorable to create a SD (4.09 eV / SD) and then have the xenon atom occupy that SD (1.06 eV / atom).[3]. SDs have more vacant space than an interstitial for the large xenon atoms, which roughly occupy the uranium position of the SD, and subsequently create less strain. A possible mechanism for xenon to diffuse in the SD is the xenon atom swaps sites with a neighboring uranium atom. However, the volume of a Schottky defect cluster (the volume of UO_2 primitive cell) is about 42 $Å^3$, very close to the van der Waals volume of xenon,[6] meaning there while the SD is more accommodating of xenon than an interstitial, there is not much space for movement of the xenon atom in a SD. Therefore, it is likely that SDs are too small to be solely responsible for xenon diffusion.[7,8, 9]

The number of vacancies required for xenon diffusion or the mechanism by which the xenon-vacancy complex diffuse is not known experimentally. Because of the difficulty of measuring atomic scale properties, calculating these properties in UO_2 has been of interest using both Density Functional Theory (DFT) [7,10,11,12,13,14,15,16,17,18,19] as well as empirical potentials. [8,9,11,12, 19,20,21,22,23] Several theoretical investigations of xenon in UO_2 have studied diffusion via a tetravacancy (TV, 2 V_U + 2 V_O) mechanism.[7,8,9] These previous investigations have proposed a variety of diffusion pathways for xenon using empirical potentials, Nudged Elastic Band (NEB), and constrained relaxations. While overall xenon transport in UO_2 has a large activation energy, that barrier can be attributed to uranium vacancy migration within the defect cluster rather than xenon migration. Grimes et al.[9] showed that xenon migration within a TV (XeTV) has a lower barrier than uranium migration, and therefore, uranium migration is the limiting factor for xenon transport. Yun et al.[7] proposed that xenon would be immobile in a Schottky defect until a (second) uranium vacancy approached the xenon-Schottky defect cluster. The xenon atom could move from the first uranium vacancy to the second, leaving the first uranium vacancy to

dissociate from the SD. In this way, xenon diffusion would be dependent on isolated uranium vacancy diffusion. Govers et al.[8] proposed that for xenon to diffuse it would occupy a tetravacancy and the xenon-tetravacancy complex would diffuse together through the "migration of the whole cluster." The xenon atom could hop between the two uranium vacancies and then the empty uranium vacancy could diffuse to a new site (still neighboring the xenon), yielding net motion of the defect.

Anderson et al.[18] have addressed the problem of xenon diffusion in UO_2 using DFT. They calculate xenon diffusion in a Xe_{U_2} defect, as an approximation for xenon in a tetravacancy because they were unable to achieve reliable barriers for Xe_{U_2O} or $Xe_{U_2O_2}$ clusters. They find a pathway similar to that of Govers et al. (Ref. 8), with barriers between 3.64 and 6.56 eV, depending on several factors (Jahn-Teller distortion, charged/neutral calculation, and supercell size). All of these previous computational studies have found that xenon migration between uranium vacancies has a small barrier compared to uranium vacancy migration and that the migration of the uranium vacancies is the rate limiting step.

More recently, Liu et al.[19] used a wholly different migration pathway for xenon in UO_2: they calculated the barrier of xenon with DFT in the thermodynamically unstable interstitial position. In this pathway, xenon moves from the interstitial site into an oxygen position, displacing an oxygen atom. This oxygen atom moves to a neighboring oxygen site, displacing a second oxygen atom. This second oxygen atom then occupies an interstitial site. The barrier from DFT is 1.6 eV, much lower than the experimental diffusion barrier (neglecting the energy needed to place xenon in an interstitial).

We seek to find which, if any, of these descriptions of xenon migration is accurate. Because XeTVs are large and are difficult to converge fully with DFT+U due to computational expense, we calculate the diffusion barriers with empirical potentials. To ensure the accuracy of our calculations, we first benchmark several pair-potentials against DFT energetics for smaller defects such as Schottky defects where DFT calculations are feasible. Then we use these empirical potentials along with NEB calculations to compare the energetics of several different xenon diffusion mechanisms.

We benchmark four empirical potentials versus DFT: Arima et al.[24], Tiwary et al.[11], Morelon et al.[25], and Basak et al.[26] For notational simplicity, we refer to these potentials just by the names of the first authors of Refs 24, 11, 25, and 26.We find that the Basak and Morelon potentials compare favorably with density functional theory for the diffusion of a Schottky defect cluster so we use these potentials to calculate the XeTV diffusion barriers. For the xenon components of the potentials, we use the empirical potentials of Geng et al.[27] and Chartier et al.,[28] which have been created to add xenon interactions to the Basak and Morelon potentials, respectively. We observe a previously unreported path for xenon-tetravacancy migration using molecular dynamics with the Basak/Geng potential. This path has a lower energy barrier than all previously reported xenon-tetravacancy paths. We examine the possibility of a uranium vacancy dissociating from the xenon-tetravacancy cluster and find that once a XeTV cluster has formed, large barriers will likely keep the individual point defects bound together in a cluster. We also calculate xenon-double Schottky defect migration and find it has a comparable barrier than xenon-tetravacancy migration and the oxygen vacancies are weakly bound to the defect.

II. Methodology

A. DFT

We calculate defects in uranium dioxide, including vacancy clusters, with and without xenon atoms, using density functional theory (DFT). For DFT calculations, we use spin-polarized DFT calculations via the Vienna *Ab Initio* Simulation Package (VASP)[29,30,31,32]. We use the generalized gradient approximation of Perdew and Wang[33] with the effective +U correction of 3.99 eV[3,34] (to the uranium f states) for strongly correlated systems as described by Dudarev[35] (here, spin-orbit coupling is neglected). Our energy cutoff was 500 eV with a 2x2x2 gamma centered k-point grid. We compared our total energies with those from a Monkhorst-Pack k-point grid and found no appreciable difference from the gamma centered grid. We use 96 atom supercells. For the perfect UO_2 lattice, we used the "U-ramping" method described by Meredig et al.[36] from a value of U-J of 0 eV to 3.99 eV to ensure low energy orbital occupations were achieved in the DFT+U calculation. For defect calculations, we start from the bulk relaxed supercell and add the defects without U-ramping (only a U-J = 3.99 eV calculation), as described in Ref. 3. For UO_2, this method of defect calculation has been found to be on par with a full U-ramping calculation.[3] We use nudged elastic band (NEB) calculations[37] to find migration barriers, with 5 beads for oxygen motion and 7 beads for uranium motion. The U-ramping method is not used for the individual NEB beads, but rather, each calculation reads in the wave functions and charge densities of the initial or final configuration (whichever is closest).

B. Empirical potentials

We also calculate vacancy clusters, with and without xenon, using empirical potentials. For these empirical potential calculations, we use the Gulp code[38] to evaluate defect energies as well as

migration energies via NEB calculations. While a core-shell potential is more likely to be able to accurately replicate vibrational properties, rigid-ion potentials are able to find accurate defect energetics (see the Morelon potential below), and we are interested in defect behavior in UO_2, therefore we utilize several rigid-ion UO_2 empirical potentials: Basak,[26] Morelon,[25] Arima,[24] and Tiwary.[11] In a forthcoming paper, we perform a detailed comparison of defects with core-shell potentials.[39] The Arima potential was parameterized with room temperature compressibility and thermal expansion data to achieve good heat capacities in UO_2 (U-O and O-O: Buckingham, formal charges). The Tiwary potential was fit to DFT+U data of uranium dioxide and splined with the ZBL potential[40] for use in cascade simulations (U-O: ZBL splined to Buckingham, O-O: ZBL splined to -3rd order polynomial-$\frac{1}{r^6}$, formal charges). The Basak potential was parameterized against thermal expansion and achieves good high temperature properties (lattice parameters, thermal expansion and isothermal compressibility) in UO_2 (O-O, U-O, and U-U: Buckingham, U-O: Morse, non-formal charges). The Morelon potential was fit to experimental defect and migration energies of point defects in UO_2, which is similar to what we will be examining in this paper (O-O: Buckingham Four range, U-O: Buckingham, non-formal charges). The Morelon potential includes a Morse interaction for the U-O pair to capture the partly-covalent behavior of the uranium and oxygen ions. None of these potentials were originally formulated with Xe-O and Xe-U potentials. However, Geng et al.[27] have created Xe-O and Xe-U potentials for use with the Basak potential. The Xe-O potential was fit to DFT calculations of XeO_3 in the hypothetical Cu_3Au structure and the Xe-U was fit to the same form as Jackson et al.,[41] a Born-Meyer function, starting with the potential parameters of Jackson et al. and refining them with additional *ab initio* calculations. Chartier et al.[28] have created Xe-O and Xe-U potentials for use with the Morelon potential fit to four xenon-containing defects calculated from DFT (we note

that the Morelon and Chartier potentials were fit to quantities similar to the ones we will use to validate the potential). Additionally, in some cases we perform calculations with different combinations of these potentials (i.e. Basak UO_2 potential with Chartier xenon potentials, or Morelon UO_2 with Geng xenon potentials). We use the supercell method where the simulation cell is periodic in all three directions, so the defect is in a periodic array, but is far enough away from its images that the interactions are small. When calculating charged defects, a charge neutralizing background is added. We use supercells of 96 atoms for direct comparison with our DFT calculations and 768 atoms for xenon diffusion calculations.

Determining the correct, low-energy diffusion pathway is often difficult in solids. One could try to guess the correct pathway, but often the lowest energy pathway is not obvious and difficult to find via simple intuition. There are methods that search for low lying transition states, such as the dimer method,[42] without prior knowledge of the pathway or even the end state. However, for problems such as diffusion in UO_2, use of these methods becomes problematic: the barriers of uranium vacancy migration in the tetravacancy are large while the oxygen barriers are relatively small. Irrelevant oxygen hops would be easily found due to the low barriers and the important uranium hops would be difficult to find. There is a third option: use molecular dynamics to observe the diffusion pathway. Molecular dynamics has the same "low barrier problem", but can be run for a long time frame such that the xenon migration path is eventually observed. We use LAMMPS[43] for molecular dynamics at artificially high temperature (3000 K) for 6 ns in order to accelerate the xenon diffusion process and subsequently calculate the energetics of the MD pathway with NEB at T = 0 K to find the transition states and the barrier energies.

C. Supercell convergence

For DFT calculations, the expense of the calculation limits the size of supercell that is used. For empirical calculations, the size limit is much less severe. We perform convergence tests on the combined Basak/Geng potentials to determine how large our supercells need to be for the migration of clusters of point defects. We calculate defect binding energies and migration barriers with different supercells (from 2x2x2 conventional fluorite cubic cells with 96 atoms to 6x6x6 cells with 2592 atoms). The binding energies are also calculated using the Mott-Littleton technique.[44] In the Mott-Littleton technique, the calculation is divided by two concentric spheres. In the inner sphere, Region I, atoms are explicitly relaxed, while atoms within the second sphere, Region IIa, are assumed to only be weakly perturbed such that atoms will respond to the perturbation in a harmonic way. Outside of the second sphere, Region IIb, the atoms extend infinitely, but are not explicitly calculated.

Point defects calculated with empirical potentials are often calculated using the Mott-Littleton technique to calculate defects in the dilute limit,[22] so we compared our supercell energetics with the Mott-Littleton energetics to ensure proper convergence. Figure 1 shows binding energy of a uranium vacancy to a xenon-Schottky defect cluster. The binding energies from largest supercell and the largest Mott-Littleton calculations agree within 0.57%, showing that the periodic images of the supercell technique have negligible interactions. The binding energy is converged within 31 meV/defect (0.9%) for the 4x4x4 supercell with respect to the 6x6x6 supercell while 2x2x2 supercell is under-converged by 228 meV/defect (6.6%). We calculated migration barriers of a xenon-tetravacancy cluster with a 4x4x4 and 6x6x6 supercell (a detailed description of this pathway is below). The two supercells have nearly identical barriers and differ by only 155 meV/defect (3.3%) at the highest barrier. A 4x4x4 supercell calculation of these defects is reasonably converged and will allow for accurate calculations of many different defects. A 2x2x2

supercell, equivalent in size to our largest DFT calculation, was small enough that the interaction of the defect with its images caused issues with the convergence of the NEB calculations.

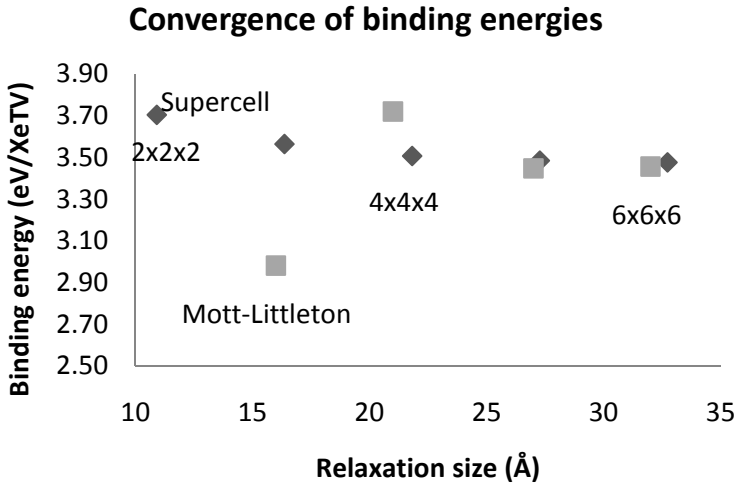

Figure 1: Convergence of binding energy of V_U to Xe_{SD}. The supercell method is tested along with the Mott-Littleton method. The Mott-Littleton is often used to calculate defect energetics in the dilute limit for empirical potentials, but the supercell technique proves to be as reliable. The relaxation size corresponds to the size of the calculation that is being explicitly relaxed: the supercell lattice parameter for pure UO_2 in the supercell method and the Region I radius for the Mott-Littleton technique. For the Mott-Littleton calculations, the Region IIa radius is the Region I radius plus 11Å. We find that a 4x4x4 supercell (768 atoms, a_0 = 21.82 Å) is sufficiently converged for binding energetics. For 2x2x2 supercells (96 atoms, a_0 = 10.91 Å), equivalent in size to our largest DFT calculation, the binding energy is overestimated by 0.2 eV.

III. Results

A. Benchmarking Pair-Potentials against DFT energetics

We begin by comparing empirical potential energetics with DFT energetics for a series of defects and migration barriers in UO_2. We have recently performed an extensive study of noble gas atoms and Schottky defects in UO_2 using the DFT+U methodology[3] (we will refer to these DFT+U calculations throughout this paper simply as DFT calculations). While these DFT

calculations are able to give insight into small, simple defects in UO_2, a well converged calculation of more complex defects (as in this paper) requires larger supercells. which can be computationally prohibitive. As discussed above, xenon is too large to diffuse in a Schottky defect and migration in UO_2 requires a tetravacancy. While a tetravacancy can be calculated within the limitations of DFT, we will show that the diffusion pathway is quite spatially extended and therefore impractical to calculate within DFT. Empirical potential calculations can accommodate the large supercell necessary for well converged defect energetics, but lack the predictive power of DFT calculations. So to bridge this gap between empirical potentials and DFT, we compare small, simple defects using both DFT and empirical potentials in order to find which empirical potentials (if any) are in energetic agreement with our DFT calculations. We then use the best potential(s) instead of DFT for spatially extended calculations where DFT would be computationally prohibitive.

We compare DFT with UO_2 potentials from Arima[24], Tiwary[11], Morelon[25], and Basak[26]. We first calculate the diffusion path of a Schottky defect with both methods. The geometry of the cluster can be defined by the positions of the two oxygen vacancies: 1st, 2nd, or 3rd nearest neighbors, relative to each other (we refer to these geometries as SD1, SD2, and SD3 respectively). The Schottky defect can transition from SD1 to SD2, as well as from SD2 to SD3 via the migration of an oxygen atom. However, these transformations are not sufficient for diffusion of a SD. In order for the empty Schottky defect to diffuse throughout the lattice, a uranium hop can transform SD1 into another SD1 via motion of the uranium atom (and, hence, the uranium vacancy) between the two oxygen vacancies. We calculate the migration of SD1 → SD1' (V_U hop), SD1' → SD2 (V_O hop), and SD2 → SD3 (V_O hop) using both DFT and empirical potentials.

Figure 2 shows the diffusion path of the constituent defects in the Schottky defect cluster. Table 1 shows the migration barriers along this pathway of Schottky defect migration calculated with DFT+U and the empirical potentials, relative to the lowest energy configuration. The lowest energy configuration for DFT, Basak, Morelon, and Arima was SD2 and for Tiwary was SD1. Because the limiting step for xenon diffusion in UO_2 is the uranium vacancy migration, it is most important that the potential agrees with DFT for the uranium barrier. Both DFT and the empirical potentials find that the barrier of oxygen vacancy migration is much smaller than the uranium barrier. Relative to the DFT calculated barriers, the Arima potential overestimates the uranium and oxygen barriers significantly and the Tiwary potential underestimates the barriers. Both the Morelon and the Basak potentials give good agreement with DFT for the uranium vacancy barrier for SD motion (the Morelon potential was fit to point defect energetics and barriers and unsurprisingly performs well); therefore, we will use the Basak and Morelon potentials to calculate the XeTV diffusion in UO_2 rather than the computationally expensive DFT.

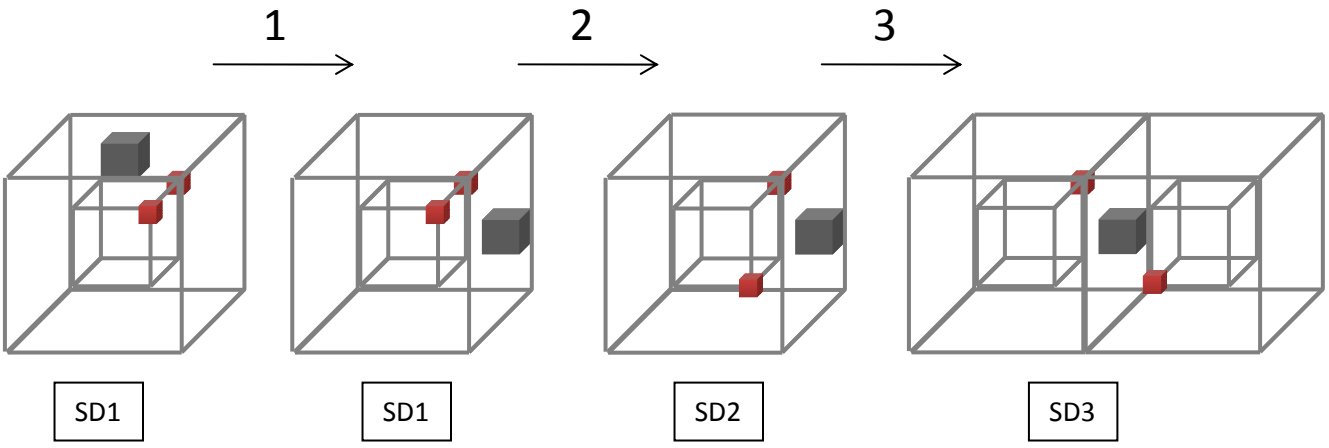

Figure 2: Migration path of a Schottky defect cluster. Only vacancies are shown. The large wireframe cube is a single unit cell of UO_2 and the inner wireframe cube corresponds to the oxygen atom positions. The gray cubes are V_U and the small red cubes are V_O. Hop 1 corresponds to a uranium vacancy hop (SD1 → SD1), hops 2 and 3 correspond to an oxygen vacancy hop (SD1 → SD2 and SD2 → SD3, respectively).

Table 1: Relative formation energies of Schottky defects and migration barrier energies from DFT+U and empirical potential NEB calculations, calculated with 93 atoms. The formation energies are relative to the lowest energy SD configuration. Hop 1 corresponds to a uranium vacancy hop (SD1 → SD1), hops 2 and 3 correspond to an oxygen vacancy hop (SD1 → SD2 and SD2 → SD3, respectively). The Arima potential overestimates all barrier energies when compared to DFT+U. The Tiwary potential underestimates all of the barrier energies. The Morelon and Basak potentials have good agreement with the DFT+U uranium diffusion barrier. The Morelon potential, which was fit to experimental defect energetics and migration barriers, agrees well with DFT+U for both the barrier heights as well as the defect energetics.

Schottky defect barriers for DFT+U and empirical potentials

Configuration	DFT+U	Arima[24]	Tiwary[11]	Morelon[25]	Basak[26]
Defect formation energies (eV/defect)					
SD1	0.76	2.10	0.00	0.69	1.79
SD2	0.00	0.00	0.71	0.00	0.00
SD3	0.12	0.38	0.69	0.00	0.32
Barrier height w.r.t. lowest energy defect (eV/defect)					
1) U Hop	5.88	12.43	3.15	5.83	6.72
2) O Hop	1.77	3.77	1.29	2.00	2.14
3) O Hop	1.34	3.76	1.32	1.92	1.96

B. Diffusion of Xe_U and Xe-Schottky Defect

Although these UO_2 potentials were not developed with a xenon component, Chartier[28] and Geng[27] created Xe-U and Xe-O potentials for the Morelon and Basak potentials, respectively, which enables the calculation of xenon in UO_2. Firstly, we check the assumption that xenon is unable to diffuse with only a single uranium vacancy.[5] We calculated possible pathways of xenon diffusion both in a single uranium vacancy and in a Schottky defect, using the nudged elastic band method with the Basak/Geng and Morelon/Chartier potentials. We calculated an exchange between the xenon atom and a neighboring uranium ion. The barrier for the exchange is over 12 eV for Basak/Geng and 7 eV for Morelon/Chartier, rendering xenon in these defects

essentially immobile with respect to thermally activated diffusion. Xenon is so large that diffusion is very difficult without a second uranium vacancy[9] needed to create a tetravacancy (TV).

C. Diffusion of Tetravacancy and Xe-Tetravacancy

Because xenon is immobile in a single uranium vacancy or even a SD, we next turn to the calculation of diffusion barriers for the migration of a xenon-tetravacancy cluster. Since vacancy clusters, like tetravacancies, have many possible configurations and component hops for the cluster to move, we must carefully define a migration energy. For each pathway considered, we define the migration energy (E_b) as the transition state of the largest barrier, E_{TS}^{Peak}, with respect to the energy of the lowest energy configuration of the vacancy cluster, E_{LE}.

$$E_b = E_{TS}^{Peak} - E_{LE} \quad (1)$$

In our calculations of xenon diffusion, we assume that the material has already been damaged by the creation of xenon atoms such many small vacancy clusters (SD, TV, etc.) exist in the material. With interatomic potentials, we cannot determine the thermodynamically preferred trap site because there is no unambiguous way to calculate the formation energy of charged defects.[8] Therefore, we do not consider the formation energy of these defect clusters and cannot compare directly with experimental activation energies, but rather can only distinguish pathways by which has the lowest barrier according to Eq. (1).

We examine pathways for TV migration with and without xenon present. In the TV and the XeTV, we have enumerated the possible oxygen vacancy configurations around two nearest neighbor uranium vacancies and found for the lowest energy configuration, the oxygen vacancies are located between the uranium vacancies. An intuitive pathway for uranium vacancy diffusion

within the TV and XeTV is for one uranium vacancy to hop directly to a different nearest neighbor position relative to the second uranium vacancy. This pathway was suggested by Govers et al. for the XeTV[8], and we call this the direct path. Figure 3 shows the direct path for the XeTV and the corresponding energetic barriers. For the XeTV, the xenon atom roughly occupies the uranium vacancy position for Basak/Geng and is halfway between uranium vacancies for Morelon/Chartier. Without xenon, the energetic barrier of the direct path is 3.0 eV for the Basak/Geng potential and 4.0 eV Morelon/Chartier potential, but when xenon is added to the tetravacancy, the barriers increase, somewhat dramatically, to 5.6 eV for both sets of potentials. This direct path migration barrier is quite large, suggesting that there is a lower energy pathway for migration energy of xenon.

To investigate novel low energy pathways, we have used molecular dynamics to evolve xenon in a TV over time using the Basak/Geng potential. Molecular dynamics is not viable for xenon diffusion over long distances because the barriers are so large that they are infrequently overcome. To accelerate the xenon diffusion process we use an artificially high temperature (3000 K). Even at this high temperature a hop of the uranium vacancies in the XeTV is rare; however there were a small amount of hops observed. In the molecular dynamics simulation, we find a new, previously-unsuspected diffusion pathway: the uranium vacancy begins in a first nearest neighbor position with respect to the xenon atom. The uranium vacancy partly dissociates from the TV by hopping to a second nearest neighbor position. Instead of fully dissociating from the TV, the uranium vacancy then hops to a new first nearest neighbor position with respect to the xenon atom. We call this new pathway the indirect pathway, and we use nudged elastic band calculations of this indirect pathway to determine the migration barriers. However, because of the extended nature of this pathway, well converged DFT calculations of this pathway are not

practical so we focus on empirical potential calculations. Figure 4 shows the indirect pathway for the XeTV and the energetic barriers of each of the component hops. The largest barriers correspond to the migration of the uranium vacancies, while the oxygen and xenon barriers are much smaller. In contrast to the direct pathway, adding xenon only slightly increases the diffusion barriers. The barrier is 4.2 eV without xenon and 4.5 eV with xenon for the Basak/Geng potential. This new pathway is very different from the path proposed by Andersson et al.,[18] which only had a single uranium hop. The indirect pathway also differs from the mechanism proposed by Yun et al.[7] in that the empty uranium vacancy need not diffuse away from xenon atom. This new indirect pathway barrier is significantly lower than that of the previously-proposed direct pathway when xenon is present (by 0.9 eV Basak/Geng, 0.5 eV Morelon/Chartier).

Interestingly, the presence of a xenon atom greatly affects the barrier for the direct pathway while the indirect pathway is comparatively unaffected. There are a few possible reasons that the addition of a xenon atom could change which pathway is more energetically favorable. For the direct path, the diffusing uranium atom comes closer to the xenon atom than for the indirect pathway. The difference in barrier energies between the two pathways could be caused by the Xe-O and Xe-U interactions being stronger for the direct pathway. The difference could also be attributed to electrostatic interactions or even interactions among uranium and oxygen atoms (U-O, U-U, and O-O interactions). In the next section, we consider separately each of these various contributions.

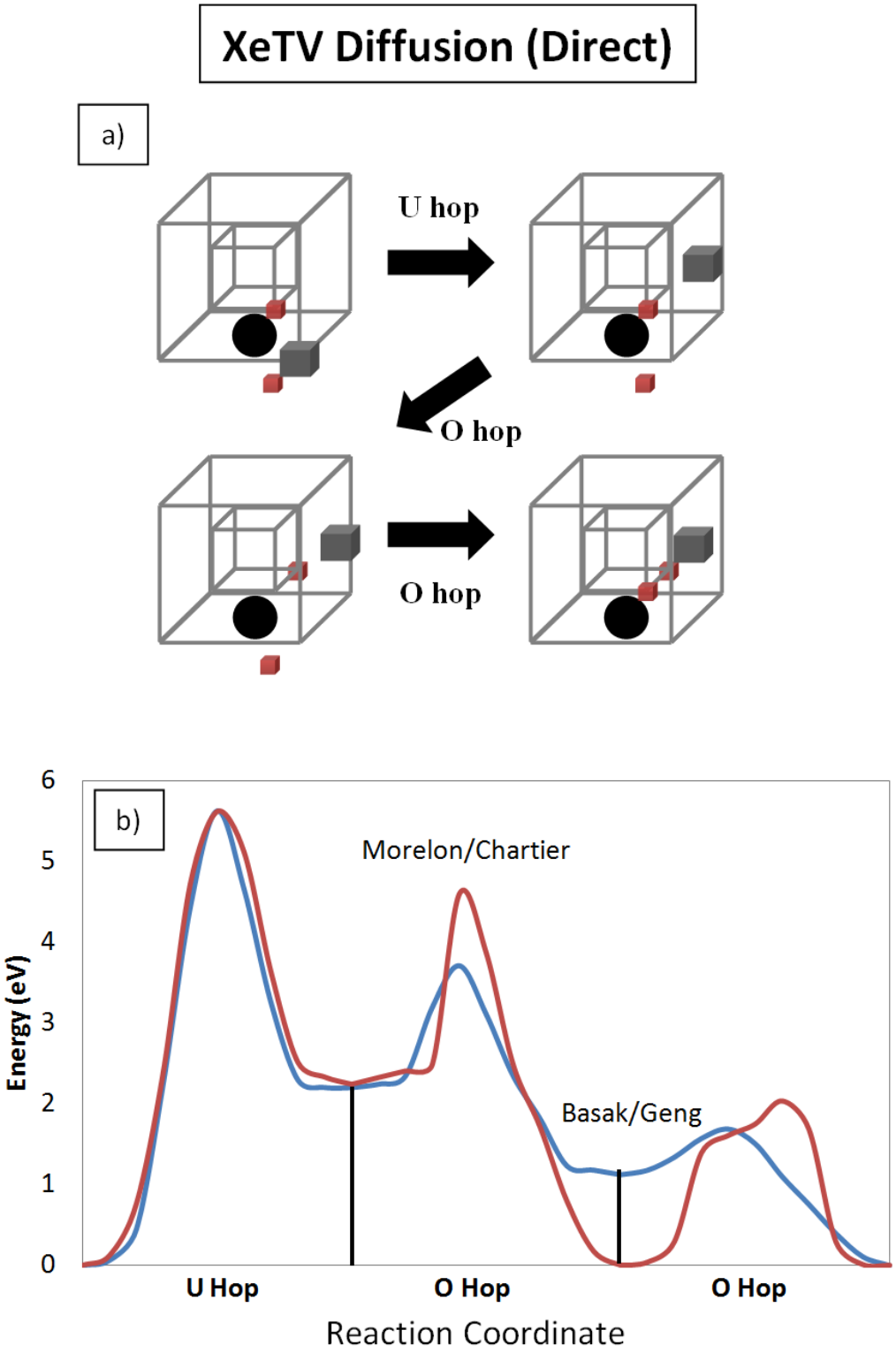

Figure 3. (a): Xenon-tetravacancy migration in UO_2 along the direct pathway. The black spheres are Xe_U, the gray cubes are V_U, the small red cubes are V_O. The large wireframe cube is a single

unit cell of UO_2 and the inner wireframe cube corresponds to the oxygen atom positions. The uranium vacancy hops directly from a nearest neighbor position to xenon to a second nearest neighbor position to xenon. Two oxygen vacancies hop and the defect returns to its original configuration. The oxygen hops experience a complicated potential landscape. The xenon atom roughly occupies the uranium vacancy position for Basak/Geng and lies directly between uranium vacancies for Morelon/Chartier. (b): The energy barriers of xenon-TV migration. The largest barrier corresponds to uranium migration (5.6 eV). Below, we find that the Basak potential has a small metastable state for uranium motion at the where the uranium is in an interstitial. The interstitial position is not stable for this path.

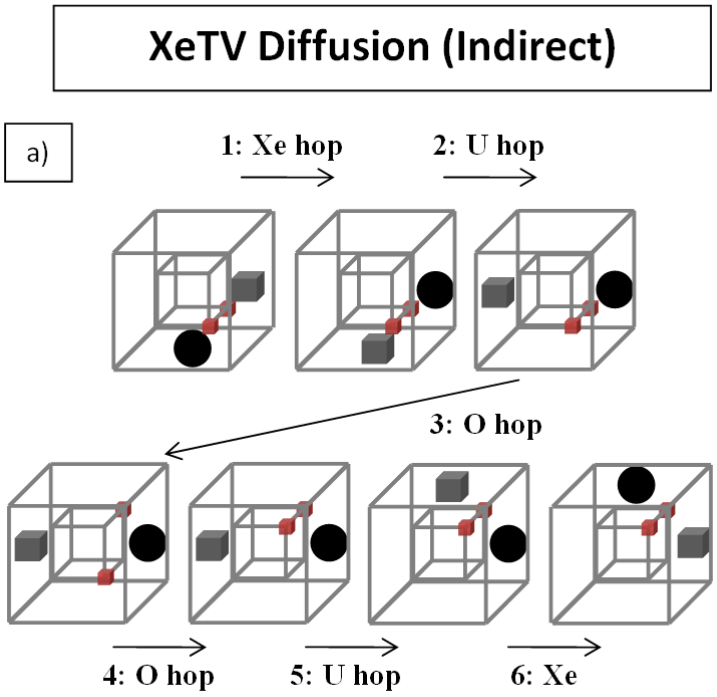

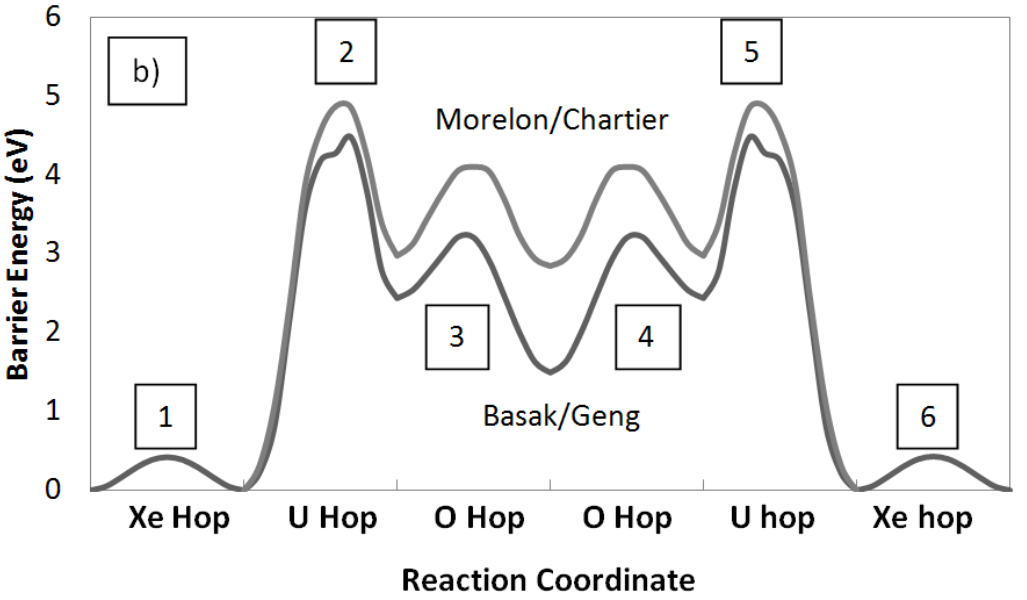

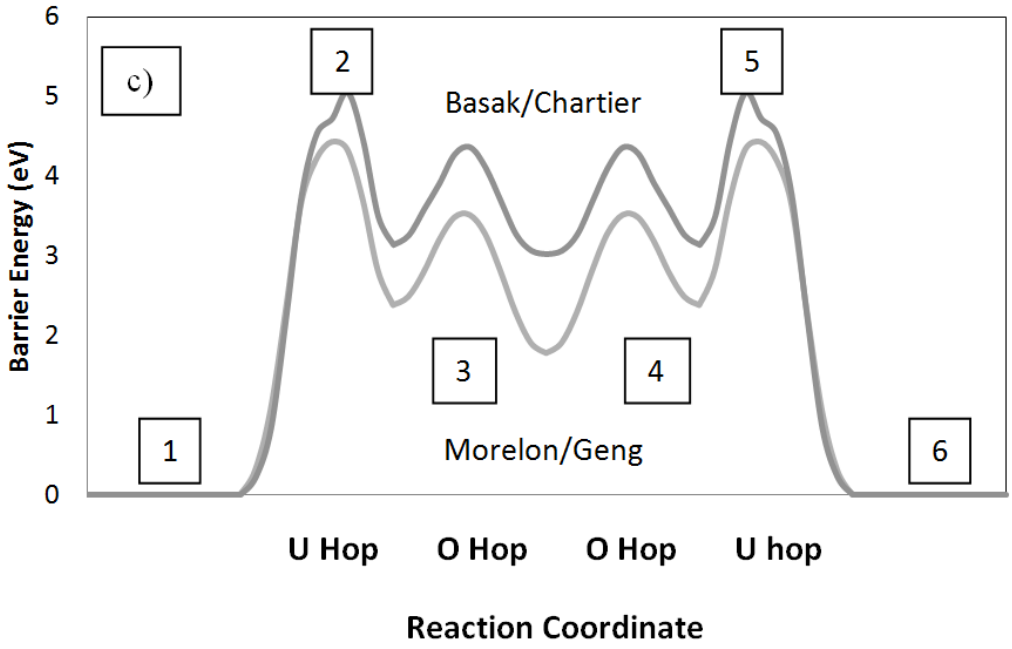

Figure 4: (a): Xenon-tetravacancy migration in UO_2 along the indirect pathway. The black spheres are Xe_U, the gray cubes are V_U, and the small red cubes are V_O. The large wireframe cube is a single unit cell of UO_2 and the inner wireframe cube corresponds to the oxygen atom positions. (1) xenon moves from one uranium vacancy to the other, (2) the uranium vacancy hops to a second nearest neighbor position, (3&4) the oxygen vacancies rearrange, (5) the uranium vacancy moves to a new first nearest neighbor position, and (6) xenon can move into

the empty uranium vacancy. (b): The energy barriers of xenon-TV migration for the Basak/Geng and Morelon/Chartier potentials. The xenon barriers are very small (Basak/Geng: 0.5 eV, Morelon/Chartier: no barrier) and the largest barrier corresponds to uranium migration (Basak/Geng: 4.5 eV, Morelon/Chartier: 4.9 eV). The oxygen vacancy steps have small barriers. The dip in the uranium hops correspond to uranium occupying an interstitial position which is a small local minimum. (c): The energy barriers of xenon-TV migration for the Morelon/Geng and Basak/Chartier potentials. The xenon atoms are located between uranium vacancies, so there are no barriers. The differences in the energies between the potentials are largely due to the different xenon potentials (Geng and Chartier) rather than the UO_2 potential.

D. Energetic components of diffusion barriers

We next examine the energetic components (electrostatic and different pair interactions) of the calculated Basak/Geng XeTV barrier energies in order to better understand the physical contribution to migration barriers. We analyze the energetics of the barriers by examining the component energies that make up the barrier: electrostatic (E_m^e), xenon interactions (E_m^{Xe}), and uranium and oxygen interactions ($E_m^{UO_2}$). The sum of these three energetic contributions is the full migration barrier energy, E_b.

$$E_b = E_m^e + E_m^{Xe} + E_m^{UO_2} \quad (2)$$

Figure 5 shows the components of the migration barriers of the direct and indirect pathways, with and without xenon present. The presence of xenon causes the direct pathway to have larger unfavorable electrostatic interactions in transition state. For the indirect pathway, adding xenon incurs a small electrostatic penalty while the U-O and O-O interaction decreases a small amount. The diffusing uranium atom moves closer to the xenon in the direct pathway, which would increase the xenon interaction energy, but the xenon interactions are the smallest component for both pathways. Rather than being a direct result of Xe-O and Xe-U interactions, the indirect pathway is lower in energy when xenon is present because of the very large electrostatic penalty

for the direct pathway. The unfavorable XeTV direct pathway is due to the fact that the presence of xenon alters the path of the diffusing uranium atom such that the configuration at the transition state is distorted from the ideal, fluorite positions, causing unfavorable electrostatic interactions.

Surprisingly, xenon does not have a large impact directly in the energetics of the pathway but rather has an indirect effect, namely the addition of xenon causes the other contributions to change drastically for the direct pathway. Having found the barrier energies and physical contributions to diffusion, we next examine the binding of the XeTV cluster. Depending on the binding of the cluster, it may either diffuse in a concerted way or the vacancies may dissociate from the xenon atom, rendering it immobile.

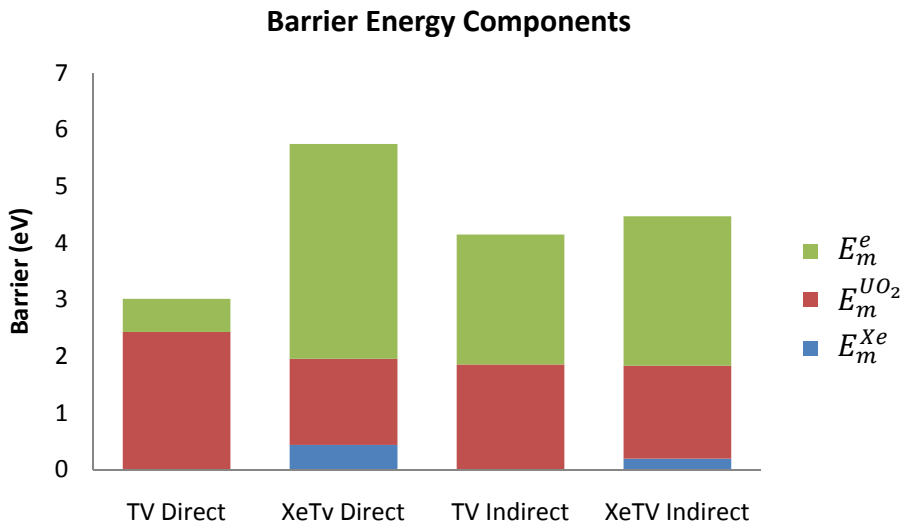

Figure 5: The components of the empirical potential energies for the TV and XeTV migration calculated with the Basak/Geng potential. We examine the energetic components of the largest energy bead from the NEB calculations. Overall, electrostatics tend to dominate the barrier heights. Adding xenon to the empty TV has different effects for the two pathways. For the direct pathway, adding xenon incurs a very large electrostatic penalty. For the indirect pathway, adding xenon incurs a smaller electrostatic penalty than the direct pathway, and the energy of the empirical potential actually decreases. The indirect pathway is lower in energy for when xenon is present because of the very large electrostatic penalty for the direct pathway.

E. XeTV Binding Energy

The two uranium vacancies in a TV cluster allow xenon to hop from one uranium site to another, but if the vacancies in the cluster are not strongly bound together, one uranium vacancy may dissociate from the TV, leaving xenon immobile as a XeSD until another uranium vacancy joins the cluster. To quantify how strongly each component of the XeTV is held together, we calculate their binding energies, E^b. When a point defect is removed from the XeTV (either a vacancy or a xenon atom), the defect cluster that remains is different for each component removed; for a uranium vacancy it is a xenon-Schottky defect cluster, for an oxygen vacancy it is a Xe_{U_2O}, and for a xenon atom it is an empty TV. For example, to determine how difficult it is to remove a uranium vacancy from a XeTV, we consider the formation energy of the constituent defects: XeTV ($Xe_{U_2O_2}$), XeSD (Xe_{UO_2}), and a uranium vacancy (V_U):

$$\boldsymbol{E^f_{Xe_{U_2O_2}} = E\left(Xe_{U_2O_2}\right) - E(bulk) + 2\mu_U + 2\mu_O - \mu_{Xe}}, \quad (3)$$

$$\boldsymbol{E^f_{Xe_{UO_2}} = E\left(Xe_{UO_2}\right) - E(bulk) + \mu_U + 2\mu_O - \mu_{Xe}}, \quad (4)$$

$$\boldsymbol{E^f_{V_U} = E(V_U) - E(bulk) + \mu_U}. \quad (5)$$

where $E\left(Xe_{U_2O_2}\right)$ and similar terms are the energies of a supercell of UO_2 with the specified defect, $E(bulk)$ is the energy of a supercell of UO_2 without any defects, and $\boldsymbol{\mu_U}$, $\boldsymbol{\mu_O}$, and $\boldsymbol{\mu_{Xe}}$ are the chemical potentials of uranium, oxygen and xenon, respectively. The binding energy of the

V_U to the Xe_{UO_2} is the difference in formation energies of those defects when they are infinitely separated and the formation energy of the defects clustered together in a $Xe_{U_2O_2}$:

$$\boldsymbol{E^b(V_U, Xe_{UO_2}) = E^f_{V_U} + E^f_{Xe_{UO_2}} - E^f_{Xe_{U_2O_2}}}, \quad (6)$$

$$\boldsymbol{E^b(V_U, Xe_{UO_2}) = E(V_U) + E\left(Xe_{UO_2}\right) - E\left(Xe_{U_2O_2}\right) - E(bulk)}. \quad (7)$$

Here, a positive binding energy indicates favorable binding. Similarly, we can define equations for the removal of an oxygen vacancy or a xenon atom:

$$\boldsymbol{E^b(V_O, Xe_{U_2O}) = E(V_O) + E\left(Xe_{U_2O}\right) - E\left(Xe_{U_2O_2}\right) - E(bulk)}, \quad (8)$$

$$\boldsymbol{E^b(Xe, V_{U_2O_2}) = E(Xe) + E\left(V_{U_2O_2}\right) - E\left(Xe_{U_2O_2}\right) - E(bulk)}. \quad (9)$$

Table 2 shows the binding energy of the constituent point defects to the xenon-tetravacancy cluster. Uranium vacancies are most weakly bound, followed by oxygen vacancies, and xenon atoms are most strongly bound. The choice of xenon potential greatly affects the binding energies. Calculations using the Chartier potential find that the binding of uranium and oxygen vacancies as stronger than calculations using the Geng potential for both the Morelon and Basak potentials. There is a large difference between the Geng and Chartier potentials for the binding energy of xenon to the tetravacancy. Essentially, the difference lies with the energetics of xenon in an interstitial. The defect energy of Xe_i calculated with the Geng potential is nearly double that of Chartier potential (Basak/Geng: 21.95 eV, Basak/Chartier: 12.84 eV, Morelon/Geng: 22.13

eV, Morelon/Chartier: 11.79 eV). The Chartier potential defect energetics are much closer to previously published DFT+U calculations for xenon in an interstitial (DFT: 9.7 eV).[3] However, because there is agreement among the UO_2-Xe potential combinations about the relative ordering of the two diffusion pathways, these xenon potentials can still find accurate migration barriers for the XeTV. We perform a comparison of xenon potentials across variety of defects in a forthcoming paper.[39]

The uranium vacancies are bound to the XeSD cluster by 2.5 eV for the Basak/Geng potential and 3.3 for the Morelon/Chartier potential. Therefore, there is a large driving force working against a uranium vacancy moving away from the rest of the xenon-tetravacancy cluster. However, after a single uranium hop away from the XeTV, as seen from Figure 4, that the energy of the XeTV is raised on the order of the binding energy of a uranium vacancy. While it appears that the vacancy has dissociated from the XeTV, this increase in energy does not mean that the uranium vacancy is fully dissociated. We need to know the migration barriers at this new position to determine if the uranium vacancy will continue to diffuse away from or if it will rejoin the XeTV.

Table 2: The binding energies of point defects to a xenon-tetravacancy cluster (Eq. 6). We use the xenon parameters from Geng and Chartier for both the Basak and Morelon UO_2 potentials in order to highlight that the differences in binding energies are largely due to the xenon potential rather than the UO_2 potential. For example, the Chartier potential increases binding energies for V_U and V_O relative to the Geng potential. The Geng potential greatly increases binding energies for Xe_i relative to the Chartier potential. All of the constituent defects of the xenon-tetravacancy were bound by at least 2.5 eV.

$E^{Binding}$ of Point defects to XeTV

Defect	Basak/Geng	Basak/Chartier	Morelon/Geng	Morelon/Chartier
V_O	3.38	4.91	3.20	3.61
V_U	2.50	4.13	2.81	3.33
Xe	17.65	8.77	17.95	8.68

F. Uranium migration away from xenon-Schottky defect

The binding energy is not the only factor for determining if a vacancy will dissociate from the rest of the cluster- migration barriers are also an important factor in considering the possibility of dissociation. Take, for example, the configuration after the first hop of the indirect pathway where the uranium vacancy is at a second nearest neighbor position to the XeSD. The uranium vacancy can hop away to *separate* from the rest of the cluster or it can hop to a first nearest neighbor position and *rejoin* the cluster. If the migration barrier for separation from the XeSD is smaller than the barrier of rejoining, the uranium vacancy would more easily migrate away from the XeSD cluster, rendering the xenon atom immobile until another (or the same) uranium vacancy approaches. If the opposite is true, the uranium vacancy will be more likely to return to the xenon-Schottky defect cluster and the xenon tetravacancy cluster would then be able to diffuse as a cluster of vacancies. Hence, we next calculate a diffusion path of a uranium vacancy away from the xenon-Schottky defect cluster.

There are many pathways for a uranium vacancy to dissociate from a XeTV, but we will limit our discussion to one example pathway. Figure 6 shows energy barriers for dissociation of a uranium vacancy from the xenon-tetravacancy. We take the first step for the dissociation of the uranium vacancy to be the same as the first step of the indirect pathway: the uranium vacancy

moves from a first nearest neighbor to the xenon atom to a second nearest neighbor. The next step for the uranium vacancy to dissociate from the rest of the XeTV (which is now a XeSD) is 3.2 eV for Basak/Geng and 3.8 eV for Morelon/Chartier. This energetic barrier is on the order of other uranium vacancy hops, however, rejoining the uranium vacancy with the XeSD has a much smaller barrier (1.7 eV for Basak/Geng, 2.0 eV for Morelon/Chartier) and therefore the uranium vacancy much more likely to rejoin the cluster. Even though the first hop of the uranium vacancy increases the energy by about the binding energy of a uranium vacancy to XeSD, this configuration is not “dissociated”.

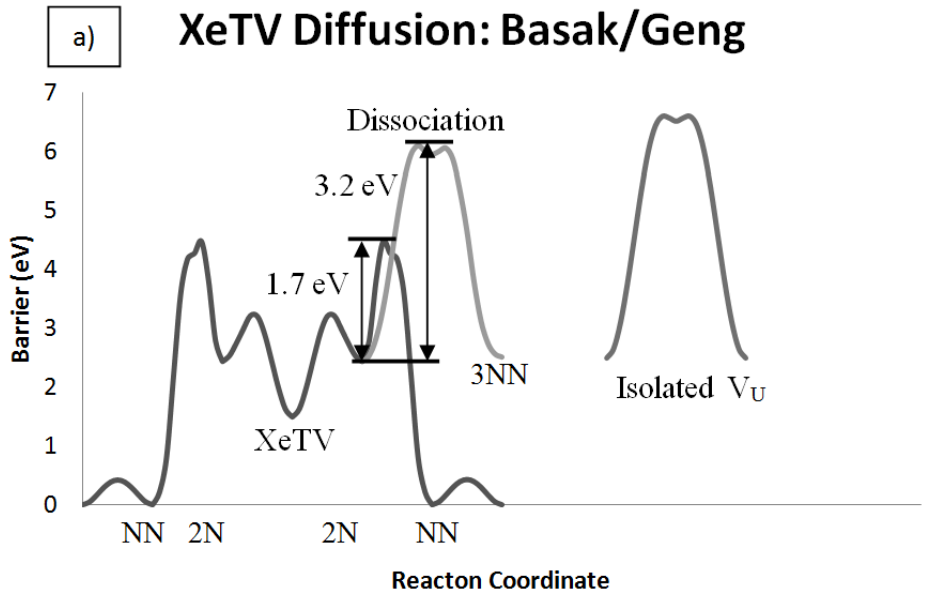

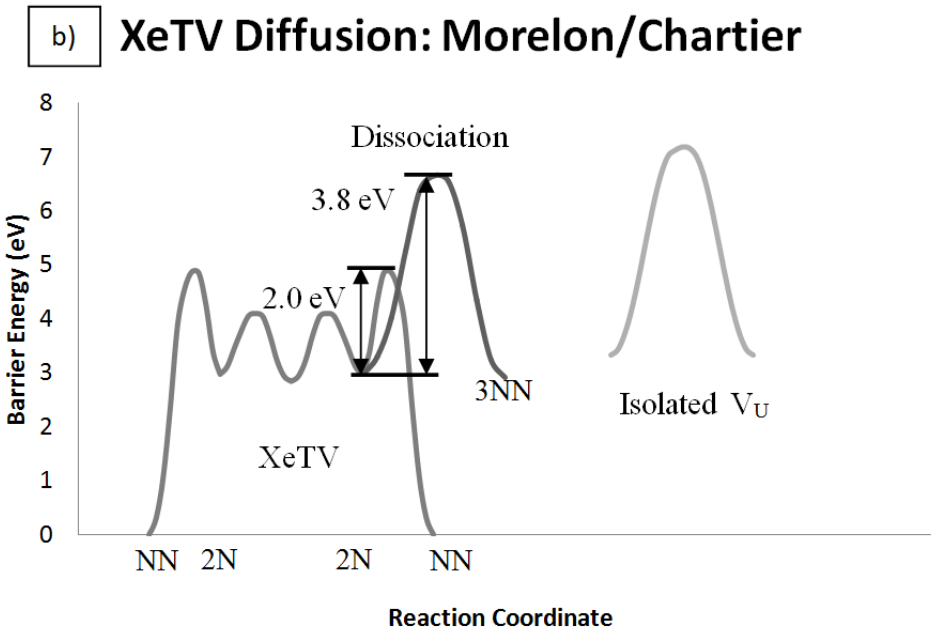

Figure 6: Energy barriers to dissociate a uranium vacancy from xenon-TV cluster for the (a) Basak/Geng potential and (b) the Morelon/Chartier potential. The diffusion barriers from Figure 4 for the self-contained diffusion of the xenon-TV cluster is shown in the bottom left corner. Additionally, a barrier is shown, starting from a metastable geometry of the diffusion process for uranium dissociation. For a sense of scale, the isolated uranium vacancy diffusion barriers are

also shown. The isolated uranium vacancy is referenced to the binding energy to XeSD. This example barrier is 1.5 eV higher than the barrier to rejoin the two defects for Basak/Geng (1.8 eV for Morelon/Chartier). The fact that the final energy of the dissociation hop is so close to the isolated uranium vacancy energy is coincidental.

G. Migration barriers of vacancy clusters

In addition to the XeTV and TV barriers, we have calculated the migration barriers of several other vacancy clusters, all containing at least one uranium vacancy, with and without xenon (see Figure 7). We begin with a discussion of uranium diffusion in the absence of xenon. Our calculated value for the migration barrier of an isolated, single uranium vacancy (4.1 eV Basak/Geng, 3.9 eV Morelon/Chartier) is larger than the experimental activation energy of 2.5 eV[45] (the activation energy will be larger than the migration barrier alone). However, the authors of Ref. 18 argue that the experimental value corresponds to a coordinated pair of uranium vacancies, which have a lower migration barrier, and that a single uranium vacancy barrier should be about 3.9-4.9 eV. This is consistent with the notion that the barrier to xenon motion is actually caused by a uranium vacancy motion. Interestingly, the migration barrier of an isolated uranium vacancy and that of a TV in the indirect pathway are roughly equivalent energetically because the uranium motion in the TV isn't aided by the second uranium vacancy. In contrast, the lowest migration barrier was the direct pathway of a TV (no xenon). This is consistent with the findings in Ref. 18 that coordinated migration of multiple uranium vacancies has a lower migration barrier than the migration of a single uranium vacancy and may be the dominant form of uranium diffusion for high concentrations of uranium vacancies.

We also calculated the barrier to migration of xenon in the smallest, mobile, charge neutral cluster of vacancies, a double Schottky defect ($Xe_{U_2O_4}$). A SD will favorably bind to a XeSD (3.8

eV for both Basak/Geng and Morelon/Chartier). We calculated 32 configurations of $Xe_{U_2O_4}$ that have two oxygen vacancies situated between the two uranium vacancies (like the low energy configuration of a TV) and the third and fourth oxygen vacancies in a nearest neighbor position to one of the uranium vacancies. We have determined the lowest energy configuration and migration configurations of the $Xe_{U_2O_4}$ are these are shown in Figure 8a. Like with the XeTV, the xenon atom roughly occupies the uranium vacancy position for Basak/Geng and lies directly between uranium vacancies for Morelon/Chartier. We used the XeTV indirect pathway as a model for the $Xe_{U_2O_4}$ path. The extra oxygen vacancies can aid uranium diffusion in the cluster if they are between the empty uranium vacancy and the second nearest neighbor site (Figure 8b). The diffusing uranium ion moves through the extra pair of oxygen vacancies. For the Basak/Geng potential, the barrier for $Xe_{U_2O_4}$ is 4.7 eV, which is close to the barrier energy for a XeTV (4.5 eV). For the Morelon/Chartier potential, the $Xe_{U_2O_4}$ barrier (4.2 eV) is smaller than the XeTV barrier (4.9 eV). The migration barriers for $Xe_{U_2O_4}$ are just above (Basak/Geng) or below (Morelon/Chartier) the XeTV barriers, however, these defects may not persist for very long. We have calculated the binding energy of the two extra oxygen vacancies in $Xe_{U_2O_4}$ and found they are less strongly bound than the oxygen vacancies that sit between the two uranium vacancies (1.6 eV Basak/Geng, 1.1 eV Morelon/Chartier). These weakly bound oxygen vacancies may dissociate and rejoin the cluster easily and could participate in the diffusion of xenon.

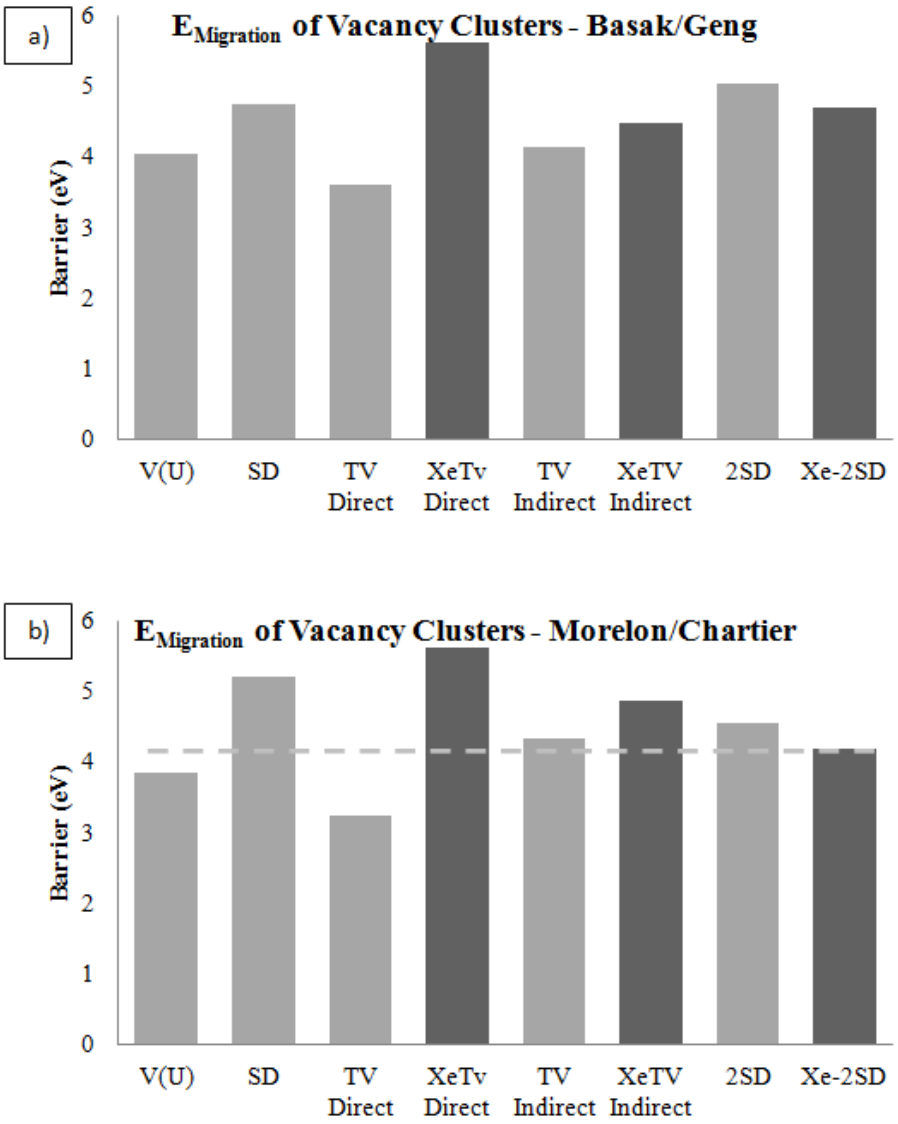

Figure 7: E_b of several mobile vacancy or xenon-vacancy clusters calculated using the nudged elastic band method with a) the Basak/Geng potential and b) the Morelon/Chartier potential. V(U) is a uranium vacancy. SD is a Schottky defect and 2SD is a double Schottky defect. The dashed line corresponds to the lowest energy barrier for a xenon containing defect. For most vacancy clusters, adding a xenon atom increased the barrier height, but this was not the case for a double Schottky defect for both potentials. For the Basak/Geng potential, the xenon migration barrier that is lowest in energy is the xenon-tetravacancy along the indirect pathway. For the Morelon/Chartier potential, the xenon-double Schottky defect has the lowest energy xenon migration barrier. Interestingly, the migration barriers of a single uranium vacancy and of a Schottky defect are larger than a tetravacancy.

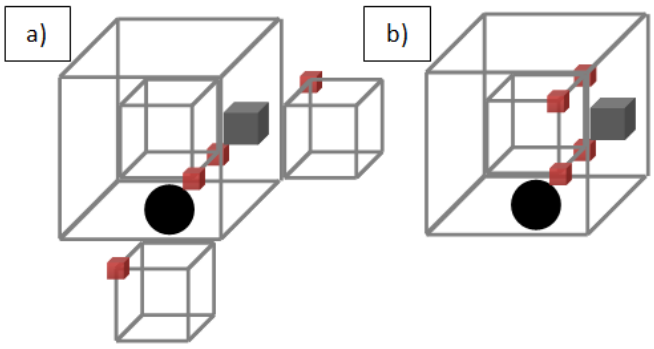

Figure 8: Xenon-double Schottky defect ($Xe_{U_2O_4}$) configurations. (a) The lowest energy configuration of $Xe_{U_2O_4}$- the vacancies lie in the same 110 plane. The configuration is similar to a XeTV with the two extra oxygen vacancies occupying sites at opposite corners of the defect. This configuration of vacancies is the lowest energy geometry of $V_{U_2O_4}$ without xenon as well. (b) The configuration modeled after the XeTV indirect pathway. Configuration (b) is 1.77 eV higher in energy than configuration (a) for Basak/Geng and 0.86 eV higher for Morelon/Chartier.

IV. Conclusions

Using a combination of Density Functional Theory (DFT), classical potentials, Molecular Dynamics (MD), and Nudged Elastic Band (NEB) calculations, we explore the diffusion pathway and migration barriers of xenon in uranium dioxide (UO_2). We perform nudged elastic band calculations to compare four empirical potentials with DFT and subsequently use two empirical potentials that agree with DFT for the calculation of xenon-vacancy clusters to determine the migration path and barrier of xenon in bulk UO_2. In our calculations, we find that the Basak and the Morelon UO_2 potentials agree qualitatively with DFT for Schottky defect diffusion. We use molecular dynamics with the Basak/Geng potential at elevated temperature to predict a new, previously-unknown xenon diffusion path in a tetravacancy. We calculate this novel pathway (indirect pathway) using nudged elastic band theory to find the migration barrier,

and we find this new pathway barrier is lower than the barrier for the previously reported xenon-tetravacancy mechanism of diffusion (direct pathway). In contrast to diffusion for xenon tetravacancies, without xenon present, the direct pathway is a lower energy pathway than the indirect pathway. Adding xenon to the tetravacancy causes a large electrostatic penalty to the direct pathway, but not the indirect pathway. We find the direct and indirect barriers are largely electrostatic and that xenon has very little direct contribution to the barrier heights. The XeTV cluster is very stable and it is difficult for a uranium vacancy to break away from the rest of the defect, making it likely that all the components of the defect will diffuse in a concerted, self contained manner. In addition to xenon diffusion in a tetravacancy, xenon can also diffuse in a double Schottky defect with comparable barrier to the XeTV. With these new pathways and barrier energetics, atomistic models for diffusion of xenon in UO_2 (such as kinetic Monte Carlo) can be used to more accurately study the mechanisms of how isolated xenon atoms diffuse and eventually coalesce into bubbles.

Acknowledgements

The authors would like to acknowledge funding from the Department of Energy under NERI-C Grant No. DE-FG07-07ID1489, and under Grant No. DE-F602-07ER46433.

References

[1] J.A. Turnbull, Journal of Nuclear Materials **38**, 203–212 (1971).
[2] W. Miekeley and F.. Felix, Journal of Nuclear Materials **42**, 297–306 (1972).
[3] A. Thompson and C. Wolverton, Physical Review B **84**, 134111 (2011).
[4] H. Matzke, Nucl. Appl. **2**, 131 (1966).
[5] D.R. Olander, *Fundamental Aspects of Nuclear Reactor Fuel Elements* (United States, 1976).
[6] A. Bondi, The Journal of Physical Chemistry **68**, 441–451 (1964).
[7] Y. Yun, H. Kim, H. Kim, and K. Park, Journal of Nuclear Materials **378**, 40–44 (2008).
[8] K. Govers, S.E. Lemehov, and M. Verwerft, Journal of Nuclear Materials **405**, 252–260 (2010).

[9] R.W. Grimes, in *Fundamental Aspects of Inert Gases in Solids*, edited by S.E. Donnelly and J.H. Evans (Springer, New York, New York, 1990), p. 415.
[10] F. Zhou and V. Ozolins, Phys. Rev. B **80**, 125127–6 (2009).
[11] P. Tiwary, A. van de Walle, and N. Grønbech-Jensen, Phys. Rev. B **80**, 174302 (2009).
[12] P. Tiwary, A. van de Walle, B. Jeon, and N. Grønbech-Jensen, Phys. Rev. B **83**, 094104 (2011).
[13] B.E. Hanken, C.R. Stanek, N. Grønbech-Jensen, and M. Asta, Physical Review B **84**, 85131 (2011).
[14] M. Freyss, N. Vergnet, and T. Petit, Journal of Nuclear Materials **352**, 144–150 (2006).
[15] T. Petit, in *Fission Gas Behaviour in Water Reactor Fuels* (OECD Publishing, Cadarache, France, 2002), p. 269.
[16] Y. Yun, O. Eriksson, and P.M. Oppeneer, Journal of Nuclear Materials **385**, 510–516 (2009).
[17] Y. Yun, O. Eriksson, and P.M. Oppeneer, Journal of Nuclear Materials **385**, 72–74 (2009).
[18] D.A. Andersson, B.P. Uberuaga, P.V. Nerikar, C. Unal, and C.R. Stanek, Phys. Rev. B **84**, 054105 (2011).
[19] X.-Y. Liu, B.P. Uberuaga, D.A. Andersson, C.R. Stanek, and K.E. Sickafus, Appl. Phys. Lett. **98**, 151902 (2011).
[20] B. Jeon, M. Asta, S.M. Valone, and N. Grønbech-Jensen, Nuclear Instruments and Methods in Physics Research Section B: Beam Interactions with Materials and Atoms **268**, 2688–2693 (2010).
[21] R.W. Grimes and C.R.A. Catlow, Philosophical Transactions of the Royal Society of London. Series A: Physical and Engineering Sciences **335**, 609–634 (1991).
[22] K. Govers, S. Lemehov, M. Hou, and M. Verwerft, Journal of Nuclear Materials **366**, 161–177 (2007).
[23] K. Govers, S. Lemehov, M. Hou, and M. Verwerft, Journal of Nuclear Materials **376**, 66–77 (2008).
[24] T. Arima, S. Yamasaki, Y. Inagaki, and K. Idemitsu, Journal of Alloys and Compounds **400**, 43–50 (2005).
[25] N.-D. Morelon, D. Ghaleb, J.-M. Delaye, and L. Van Brutzel, Philosophical Magazine **83**, 1533 (2003).
[26] C.B. Basak, A.K. Sengupta, and H.S. Kamath, Journal of Alloys and Compounds **360**, 210–216 (2003).
[27] H.Y. Geng, Y. Chen, Y. Kaneta, and M. Kinoshita, Journal of Alloys and Compounds **457**, 465–471 (2008).
[28] A. Chartier, L. Van Brutzel, and M. Freyss, Phys. Rev. B **81**, 174111 (2010).
[29] G. Kresse and J. Hafner, Phys. Rev. B **47**, 558 (1993).
[30] G. Kresse, Thesis, Technische Universität Wien, Vienna, Austria, 1993.
[31] G. Kresse and J. Furthmüller, Computational Materials Science **6**, 15–50 (1996).
[32] G. Kresse and J. Furthmüller, Phys. Rev. B **54**, 11169 (1996).
[33] J.P. Perdew, in *Electronic Structure of Solids*, edited by P. Ziesche (Akademie Verlag, Berlin, 1991), p. 11.
[34] B. Dorado, B. Amadon, M. Freyss, and M. Bertolus, Phys. Rev. B **79**, 235125–8 (2009).
[35] S.L. Dudarev, G.A. Botton, S.Y. Savrasov, C.J. Humphreys, and A.P. Sutton, Phys. Rev. B **57**, 1505 (1998).
[36] B. Meredig, A. Thompson, H.A. Hansen, C. Wolverton, and A. van de Walle, Phys. Rev. B **82**, 195128 (2010).
[37] H. JóNsson, G. Mills, and K.W. Jacobsen, in (World Scientific Publishing Co. Pte. Ltd., 1998), pp. 385–404.
[38] J.D. Gale and A.L. Rohl, Molecular Simulation **29**, 291–341 (2003).
[39] A. Thompson and C. Wolverton, In Preparation (n.d.).
[40] J.F. Ziegler, *The Stopping and Range of Ions in Solids*, First Edition (Pergamon Pr, 1985).
[41] R.A. Jackson and C.R.A. Catlow, Journal of Nuclear Materials **127**, 161–166 (1985).
[42] G. Henkelman and H. Jónsson, J. Chem. Phys. **111**, 7010 (1999).
[43] S. Plimpton, Journal of Computational Physics **117**, 1–19 (1995).
[44] N.F. Mott and M.J. Littleton, Transactions of the Faraday Society **34**, 485 (1938).
[45] H.J. Matzke, in *Diffusion Processes in Nuclear Materials* (North-Holland, Amsterdam, 1992).